Noninvasive diagnosis of mucopolysaccharidosis via depth-resolved optical spectroscopy of the outer ear

Richa Mittal, Philip H. Schwartz, David J. Brick, and Chad A. Lieber*

CHOC Research Institute, CHOC Children's Hospital, 455 South Main St., Orange, CA 92868, USA
**clieber@choc.org*

Abstract: Current diagnostics for lysosomal storage disorders such as mucopolysaccharidosis (MPS) rely on evaluation of ex vivo bodily fluids, which has several shortcomings. In this study, we evaluated whether Raman spectroscopy could noninvasively diagnose MPS in a murine model. Via confocal sampling of the murine outer ear, Raman spectra were obtained at multiple depths. Partial least-squares discriminant analysis of the processed Raman spectra showed a 93% sensitivity and 91% specificity for disease. The discriminant algorithm relied on several Raman bands related to glycosaminoglycans (GAGs) that typically accumulate in MPS. These findings indicate the possibility for a new, noninvasive diagnostic tool for MPS.

OCIS codes: (170.6510) Spectroscopy, tissue diagnostics; (170.4580) Optical diagnostics for medicine.

References

1. S. Byers, T. Rozaklis, L. K. Brumfield, E. Ranieri, and J. J. Hopwood, "Glycosaminoglycan accumulation and excretion in the mucopolysaccharidoses: characterization and basis of a diagnostic test for MPS," Mol. Genet. Metab. **65**(4), 282–290 (1998).
2. P. J. Roughley, "The structure and function of cartilage proteoglycans," Eur. Cell. Mater. **12**, 92–101 (2006).
3. J. E. Wraith, "The mucopolysaccharidoses: a clinical review and guide to management," Arch. Dis. Child. **72**(3), 263–267 (1995).
4. J. C. Fratantoni, C. W. Hall, and E. F. Neufeld, "The defect in Hurler's and Hunter's syndromes: faulty degradation of mucopolysaccharide," Proc. Natl. Acad. Sci. U.S.A. **60**(2), 699–706 (1968).
5. P. J. Meikle, M. J. Fietz, and J. J. Hopwood, "Diagnosis of lysosomal storage disorders: current techniques and future directions," Expert Rev. Mol. Diagn. **4**(5), 677–691 (2004).
6. T. Khaliq, M. Sadilek, C. R. Scott, F. Turecek, and M. H. Gelb, "Tandem mass spectrometry for the direct assay of lysosomal enzymes in dried blood spots: application to screening newborns for mucopolysaccharidosis IVA," Clin. Chem. **57**(1), 128–131 (2011).
7. C. J. Dean, M. R. Bockmann, J. J. Hopwood, D. A. Brooks, and P. J. Meikle, "Detection of mucopolysaccharidosis type II by measurement of iduronate-2-sulfatase in dried blood spots and plasma samples," Clin. Chem. **52**(4), 643–649 (2006).
8. R. Y. Wang, O. A. Bodamer, M. S. Watson, and W. R. Wilcox; ACMG Work Group on Diagnostic Confirmation of Lysosomal Storage Diseases, "Lysosomal storage diseases: diagnostic confirmation and management of presymptomatic individuals," Genet. Med. **13**(5), 457–484 (2011).
9. J. Chan, S. Fore, S. Wachsmann Hogiu, and T. Huser, "Raman spectroscopy and microscopy of individual cells and cellular components," Laser Photonics Rev. **2**(5), 325–349 (2008).
10. E. B. Hanlon, R. Manoharan, T. W. Koo, K. E. Shafer, J. T. Motz, M. Fitzmaurice, J. R. Kramer, I. Itzkan, R. R. Dasari, and M. S. Feld, "Prospects for in vivo Raman spectroscopy," Phys. Med. Biol. **45**(2), R1–R59 (2000).
11. A. Mahadevan-Jansen and R. Richards-Kortum, "Raman spectroscopy for the detection of cancers and precancers," J. Biomed. Opt. **1**(1), 31–70 (1996).
12. N. Stone, C. Kendall, N. Shepherd, P. Crow, and H. Barr, "Near-infrared Raman spectroscopy for the classification of epithelial pre-cancers and cancers," J. Raman Spectrosc. **33**(7), 564–573 (2002).
13. P. J. Caspers, G. W. Lucassen, E. A. Carter, H. A. Bruining, and G. J. Puppels, "In vivo confocal Raman microspectroscopy of the skin: noninvasive determination of molecular concentration profiles," J. Invest. Dermatol. **116**(3), 434–442 (2001).
14. C. A. Lieber and A. Mahadevan-Jansen, "Development of a handheld Raman microspectrometer for clinical dermatologic applications," Opt. Express **15**(19), 11874–11882 (2007).

#151857 - $15.00 USD Received 27 Jul 2011; revised 26 Aug 2011; accepted 29 Aug 2011; published 6 Sep 2011

15. P. Matousek, I. P. Clark, E. R. C. Draper, M. D. Morris, A. E. Goodship, N. Everall, M. Towrie, W. F. Finney, and A. W. Parker, "Subsurface probing in diffusely scattering media using spatially offset Raman spectroscopy," Appl. Spectrosc. **59**(4), 393–400 (2005).
16. N. Stone, K. Faulds, D. Graham, and P. Matousek, "Prospects of deep Raman spectroscopy for noninvasive detection of conjugated surface enhanced resonance Raman scattering nanoparticles buried within 25 mm of mammalian tissue," Anal. Chem. **82**(10), 3969–3973 (2010).
17. R. Ellis, E. Green, and C. P. Winlove, "Structural analysis of glycosaminoglycans and proteoglycans by means of Raman microspectrometry," Connect. Tissue Res. **50**(1), 29–36 (2009).
18. R. Bansil, I. V. Yannas, and H. E. Stanley, "Raman spectroscopy: a structural probe of glycosaminoglycans," Biochim. Biophys. Acta **541**(4), 535–542 (1978).
19. N. S. J. Lim, Z. Hamed, C. H. Yeow, C. Chan, and Z. Huang, "Early detection of biomolecular changes in disrupted porcine cartilage using polarized Raman spectroscopy," J. Biomed. Opt. **16**(1), 017003 (2011).
20. V. Renugopalakrishnan, S. Zheng, A. T. Tu, and S. P. Damle, "Secondary structure of pig skin proteodermatan sulfate: a perspective from Raman spectroscopic studies in aqueous solution," Biopolymers **28**(11), 1935–1938 (1989).
21. L. A. Clarke, C. S. Russell, S. Pownall, C. L. Warrington, A. Borowski, J. E. Dimmick, J. Toone, and F. R. Jirik, "Murine mucopolysaccharidosis type I: targeted disruption of the murine α-L-iduronidase gene," Hum. Mol. Genet. **6**(4), 503–511 (1997).
22. T. Pearson, D. L. Greiner, L. D. Shultz, T. Nomura, T. Watanabe, and S. Habu, *Humanized SCID Mouse Models for Biomedical Research* (Springer, Berlin, 2008), pp. 25–51.
23. M. G. Shim and B. C. Wilson, "The effects of ex vivo handling procedures on the near-infrared Raman spectra of normal mammalian tissues," Photochem. Photobiol. **63**(5), 662–671 (1996).
24. C. A. Lieber and A. Mahadevan-Jansen, "Automated method for subtraction of fluorescence from biological Raman spectra," Appl. Spectrosc. **57**(11), 1363–1367 (2003).
25. J. R. Beattie, J. V. Glenn, M. E. Boulton, A. W. Stitt, and J. J. McGarvey, "Effect of signal intensity normalization on the multivariate analysis of spectral data in complex 'real world'datasets," J. Raman Spectrosc. **40**(4), 429–435 (2009).
26. N. K. Afseth, V. H. Segtnan, and J. P. Wold, "Raman spectra of biological samples: A study of preprocessing methods," Appl. Spectrosc. **60**(12), 1358–1367 (2006).

1. Introduction

The mucopolysaccharidoses (MPS) are a family of genetic disorders within the greater umbrella of lysosomal storage diseases. These diseases are linked by a deficiency in lysosomal hydrolases that catalyze the degradation of glycosaminoglycans (GAGs). As a result, GAGs that are normally recycled in a healthy individual cannot be degraded in the MPS patient. Undegraded GAGs are accumulated in cells and can adversely affect the tissue (e.g. cartilage, bone, kidney) function [1,2]. MPS type I (MPS-I) is one of the most prevalent forms of the MPS disease, usually denoted as Hurler's syndrome in more severe manifestations and Scheie's syndrome when less severe. MPS-I is the result of a deficiency in the iduronidase enzyme, wherein the specific GAGs that accumulate in the tissues are heparin sulfate and dermatan sulfate [3,4].

Conventional methods for measuring GAG accumulation rely on patient fluids (urine or blood), which indicate systemic GAG concentrations and lack tissue specificity [5–7]. Measurement of GAGs is performed at a small number of specialty laboratories nationwide and generally requires days to weeks turnaround time, delaying diagnosis and initiation of treatment. Furthermore, systemic GAG concentrations can be unreliable for the monitoring of disease progression or efficacy of treatment; once treated with enzyme replacement therapy (ERT) or hematopoietic stem cell transplantation (HSCT), a patient's systemic GAG levels decline to near-normal levels while obvious disease progression continues in skeletal, cardiac, and other systems [8]. Based on these shortcomings, the development of a new technique for noninvasive diagnosis of MPS disease involvement and quantification of treatment response is obviously warranted.

Raman spectroscopy is an optical technique for molecular analysis that has been used extensively in various biomedical applications [9–12]. These studies have shown that Raman spectroscopy is capable of detecting subtle changes in tissue biochemistry to allow noninvasive diagnosis of pathology. More importantly, Raman spectra can be obtained at resolved depth, via standard optical modalities such as confocal [13,14] or separated source-detector [15,16], to allow the biochemical characterization of subsurface anatomic structures.

#151857 - $15.00 USD Received 27 Jul 2011; revised 26 Aug 2011; accepted 29 Aug 2011; published 6 Sep 2011

Additionally, several studies have shown that GAGs exhibit multiple distinct peaks in the Raman spectrum [17–20], which indicates the potential to detect these GAGs within the tissue milieu.

Based on the demonstrated capabilities of Raman spectroscopy and the demonstrated need for new MPS diagnostics, we evaluated in this study the Raman technique's ability to provide noninvasive diagnosis of MPS-I in a murine model. This preliminary data and previous successes in the use of Raman spectroscopy for other biomedical applications suggest that the Raman technique may provide diagnostic value in the clinical management of MPS.

2. Materials and methods

This study was performed using the MPS-I murine model described in [21] bred into a NOD-SCID-IL2Rγ (NSG) background [22]. In brief, this model is created by genetic knockout of α-L-iduronidase (IDUA), manifesting in visually apparent phenotypic response by approximately 4 weeks of age. Seven IDUA knockout mice (termed "disease" population) and five wild type mice (termed "normal" population) were evaluated as part of this study. The outer ear was clipped from the animals immediately after sacrifice for population control of an existing study, snap frozen in liquid nitrogen and stored at −80 °C until the time of optical measurement. The age and genotype of the animals studied is included in Table 1. Upon time of optical measurement, the samples were passively thawed in PBS for ~15 minutes at room temperature to avoid any spectral artifacts related to freeze/thaw [23]. Dermatan and heparan sulfates were obtained in dried, purified form (Sigma Aldrich, St. Louis, MO) and characterized on the same measurement system.

Table 1. Genotype and age (at time of sacrifice) of mice

Sample	Age (months)	IDUA genotype
1	13.8	–/–
2	9.4	–/–
3	9.4	–/–
4	7.7	–/–
5	7.5	–/–
6	4.1	–/–
7	13.8	–/–
8	13.8	+/+
9	4.1	+/+
10	13.5	+/+
11	10	+/+
12	10	+/+

Spectra were obtained using a confocal Raman microspectrometer (RM1000, Renishaw PLC, Wotton-under-Edge, UK). This system is based on an upright microscope with attached spectrometer. The laser emits in the near-infrared region (785 nm) and the sample is exposed through a 50 × , 0.55 NA objective (LMPlan IR, Olympus Corp., Center Valley, PA) with 40 mW power at the sample focused into a spot. The light was collected in the epi-direction and detected using a CCD camera with a slit aperture to maintain system confocality. Using a 100 mm slit width in the spectrometer, the spatial resolution of the system is ~2 μm laterally and ~4 μm axially, as determined by the full-width-at-half-max of the spectra obtained by scanning a 1 μm polystyrene bead in 3 dimensions.

Raman spectra were measured from the skin surface down to depth of 200 μm in increments of 20 μm. Measurements were made in randomly selected locations within the central portion of the outer ear samples, where the cross-section shows a generally uniform dimension among the strata. All spectra were obtained with a 60 second integration time in

#151857 - $15.00 USD Received 27 Jul 2011; revised 26 Aug 2011; accepted 29 Aug 2011; published 6 Sep 2011

the spectral range 600-1700 cm^{-1}. For each experiment, spectral dispersion was calibrated using a neon-argon lamp, wavenumber shift calibration was performed using acetaminophen as a reference standard, and system response was calibrated using a doped glass standard (NIST 2241). Higher frequency readout and shot noise was removed by a second-order Savitzky-Golay smoothing filter. Tissue autofluorescence was subtracted via an automated 5th order modified polynomial fitting method using the full wavenumber range [24]. The processed spectra were binned to 5 cm^{-1} and normalized to four different normalizations schemes: the mean normalized intensity of the entire spectrum (600-1700 cm^{-1}), the 1003 cm^{-1} peak (phenylalanine ring vibration) intensity, the 1443 cm^{-1} peak (CH_2 bend of proteins/lipids) intensity, and the 1658 cm^{-1} peak (Amide I stretch of proteins/lipid) intensity, all of which have been recommended based on previous comparative studies [25,26]. All normalization methods were carried through subsequent analysis.

The preprocessed spectra were analyzed using partial least squares discriminant analysis (PLSDA, PLS Toolbox Version 6.2.1, Eigenvector Research Inc., Wenatchee, WA) in the Matlab (Mathworks Inc., Natick, MA, Version R2010a) programming environment. To ensure robust results, cross validation was done using multiple (20) iterations of random subset withholding (leave 10% out). Sample scores were used to assess diagnostic accuracy of the Raman spectra, using decision lines that maximized separation of the normal and disease populations. Because there were only two classes evaluated, the calculated sensitivity and specificity values are interchangeable.

3. Results and discussion

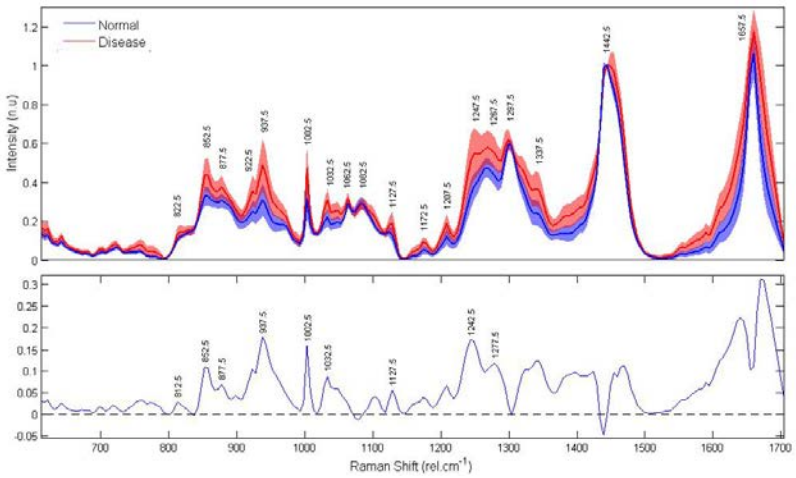

Fig. 1. Top: Mean Raman spectra of all normal and disease samples, with shaded boundary of (±) standard deviation. Bottom: Difference spectrum (disease minus normal) obtained from the mean spectra reveal a number of band differences between the populations.

The Raman spectra of both normal and disease populations are shown in Fig. 1 (normalized to CH_2 bending mode of proteins and lipids at 1443 cm^{-1}, as described below). Qualitatively, there are spectral differences between the two populations that can be more readily visualized in the difference spectra (bottom plot of Fig. 1). The most significant differences are seen in the protein and lipid Raman band regions and in the spectral features of the functional groups of disease-relevant sulfated GAGs.

The most apparent difference is observed in the increased intensity of diseased tissue amide III band region around 1240-1300 cm^{-1}, the CH_3 symmetric deformation band at 1377 cm^{-1}, the symmetric ring at 1002 cm^{-1} and C-H bending at 1032 cm^{-1} of phenylalanine [11,12]. In regions of GAG Raman activity, the spectra are most different in the glycosidic

#151857 - $15.00 USD Received 27 Jul 2011; revised 26 Aug 2011; accepted 29 Aug 2011; published 6 Sep 2011

linkage (C-O-C) vibration band at 937 cm^{-1} [18] (also attributed to C–C stretching of proline/valine amino acid), and the 822 cm^{-1} and 852 cm^{-1} peaks attributed to asymmetric vibration of the C-O-S linkage, which has also been attributed to tyrosine/proline amino acid [11,12]. There are also slight differences seen at amide I proteins and lipids band at 1658 cm^{-1}, symmetric stretch of the sulfate group ($OSO3^-$) at 1062 cm^{-1}, and C-OH deformation at 1127 cm^{-1}. The attributions of the dominant peaks in the measured spectra are summarized in Table 2, with band assignments derived from the literature. Generally, disease tissues show an increase in all major GAG vibrations as well as proline, valine, and phenylalanine amino acids, when the spectra is normalized to structural proteins and lipids (1443 cm^{-1} or 1658 cm^{-1} peaks).

Table 2. Major vibrational modes observed in normal and diseased mouse ear Raman spectra and sulfated glycosaminoglycans[a]

Band (cm^{-1})	Assignment
822	Asymmetric C-O-S linkage vibration of GAGs, Tyrosine/O–P–O stretch of DNA
852	Asymmetric C-O-S linkage vibration of GAGs, Tyrosine and C–C stretch of proline ring
877	C-H deformation for β anomers
937	Glycosidic linkage C-O-C vibration in GAGs, C–C stretch of proline/valine and protein backbone
1002	Symmetric ring of phenylalanine
1032	C–H bending of phenylalanine
1062	OSO^-_3 symmetric stretch from sulfate group of GAGs
1082	C–N stretch of proteins and lipid, and C-OH deformation
1127	C–C stretching of lipids, C–N protein stretch, C-H and C-OH deformation
1240–1300	Amide III (C–N stretch of proteins)
1337	CH_3CH_2 wagging of collagen, polynucleotide chain and phenylalanine
1443	CH_2 bending of proteins and lipids
1658	Amide I (C = O stretching of proteins), C = C lipid stretch

[a]From [11,12,18]

To illustrate the spectral dependence on measurement depth, Fig. 2 shows a depth-series-plot of the mean Raman spectra obtained from the 2 oldest animals of each population (animals 1, 7, 8, and 10; displayed depths are reduced for clarity). Epidermal measurements (surface to ~20 μm) produce relatively subtle spectral differences between the normal and diseased tissues. However, 60 μm and deeper measurements produce much more significant disparity between the population spectra, with increased intensity in the diseased tissues at all the major GAG and amino acid peaks (857, 922, 937, 1003, 1032, 1062, 1247 cm^{-1}). There is also a decreased signal at the 1658 cm^{-1} Amide I peak for diseased tissue compared to normal, as well as a possible conformational change shifting the 1443 cm^{-1} CH_2 bending mode (to ~1453 cm^{-1}). Thus, there is a discernable unique chemical process occurring in the deeper layers (dermis, cartilage) versus the superficial skin layers. This is reasonable, given the general manifestation of GAGs and associated accumulation in cartilaginous structures of the MPS patient. Morphometric analysis of a stained cross section of one of the ears studied here showed a dermal thickness (stratum corneum through dermis) of approximately 40-100 μm on both sides of a central cartilage layer of ~50 μm thickness. This finding is important for future clinical evaluations of Raman spectroscopy for MPS disease characterization, as such a clinical system will benefit from a deeper interrogation depth and possibly a combined imaging technique to allow determination of subsurface anatomy.

The PLSDA scores plot of the Raman spectra are shown in Fig. 3, which reveals a distinct difference in scattering between the two populations. On inserting a decision line between the 2 populations, 64 of 70 disease measurements and 46 of 50 normal measurements could be correctly classified, resulting in 93% sensitivity and 91% specificity for disease. Using the

#151857 - $15.00 USD Received 27 Jul 2011; revised 26 Aug 2011; accepted 29 Aug 2011; published 6 Sep 2011

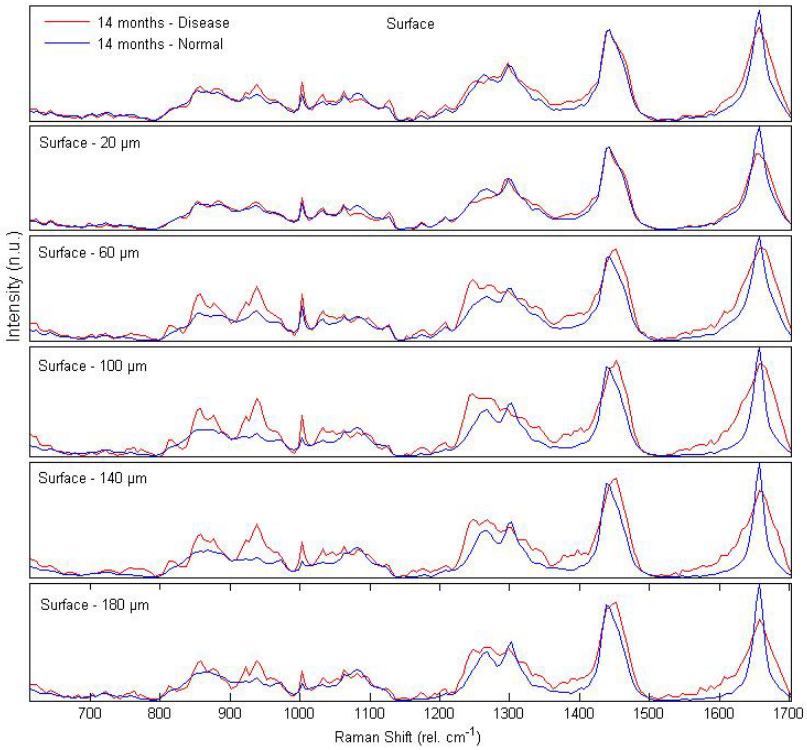

Fig. 2. Mean Raman spectra of disease and normal tissues at different measured depth. Marked differences are seen between the two tissue types at depths greater than ~60 µm.

majority diagnosis for all the spectra obtained from each animal, this translates to accurate diagnosis of 6 of 7 diseased and 5 of 5 normal animals. The 1 misclassified diseased animal in this analysis happened to be 7.5 months of age and it not clear yet the cause of this discrepancy. However, if only the measurements obtained from subdermal depths (~60 µm-140 µm) are utilized, all animals are correctly diagnosed. Indeed, all the major discrepancies in the score plot for both disease and normal populations are observed either in the superficial skin measurements or very deep in the tissue (~180 µm), where the symmetric profile of the ear cross-section would result in measurement of the opposite skin layer.

To determine which spectral features are most diagnostically relevant, the loading plots of the PLSDA were evaluated, as seen in Fig. 4. The figure also shows the Raman spectra of purified salts of dermatan and heparan sulfates, exhibiting the major Raman peaks present in the sulfated GAGs typically elevated in MPS-I for comparison. Major differences in the Raman peaks are seen at 867, 942, 977, 1062, 1082, 1122, 1237, 1342, 1412, 1657 cm^{-1}, most of which were identified in the difference spectra and attributed in Table 2. For direct comparison with the sulfated GAGs, the spectral bands of diagnostic significance are highlighted by dotted lines.

The choice of normalization scheme proved to be an important consideration, as demonstrated by previous comparative studies [25,26]. Following each scheme through discriminant analysis, normalization to the 1443 cm^{-1} peak provided maximum sensitivity and specificity (93% and 91%, respectively), followed closely by normalization to the 1658 cm^{-1} peak (92% and 90%) and mean (87% and 92%), while 1003 cm^{-1} peak normalization yielded a much poorer performance (84% and 75%). Qualitatively, the schemes based on the dominant 1443 and 1658 cm^{-1} bands resulted in an overall elevation of the GAG bands in

#151857 - $15.00 USD Received 27 Jul 2011; revised 26 Aug 2011; accepted 29 Aug 2011; published 6 Sep 2011

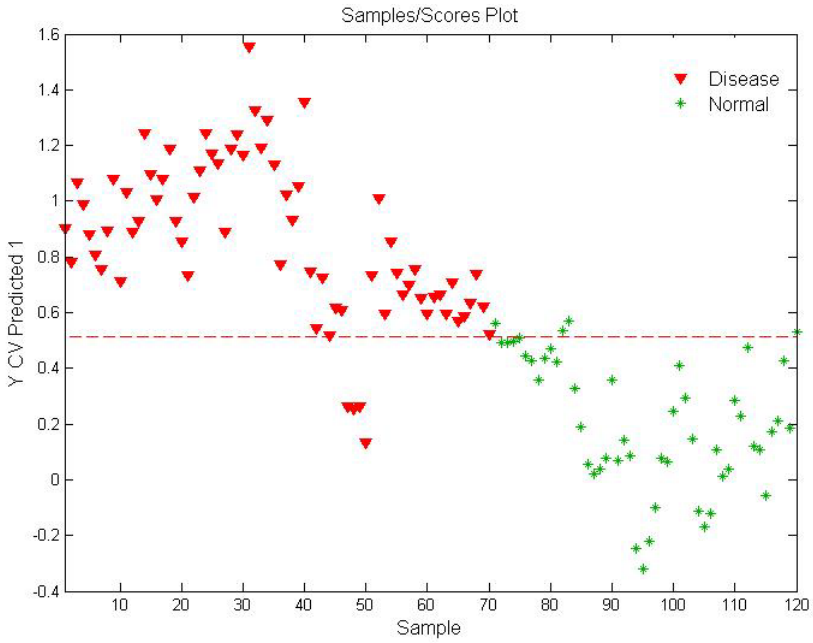

Fig. 3. Discriminant function scores (from PLSDA) for all measured spectra, showing a separation of the two populations with 93% sensitivity and 91% specificity.

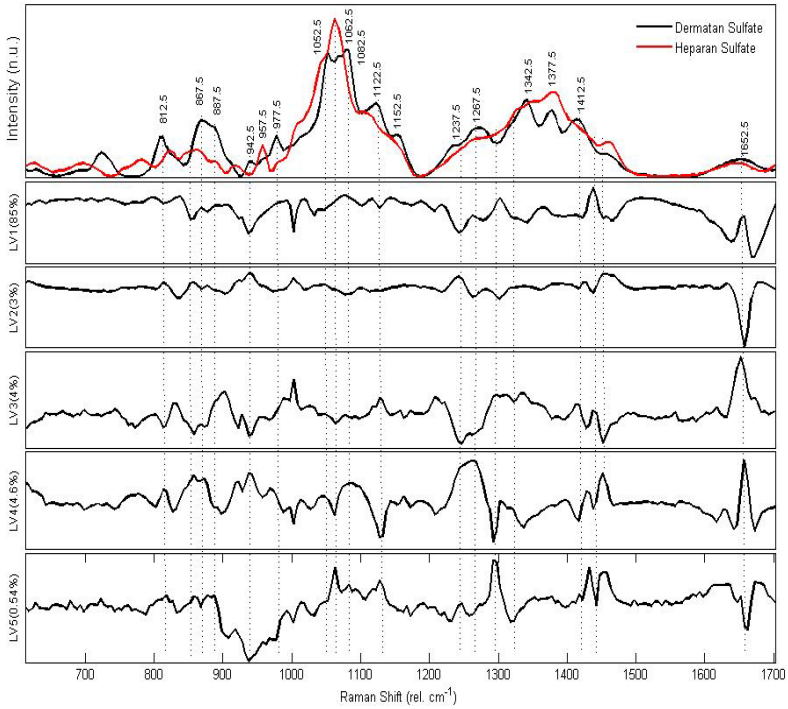

Fig. 4. (Top) Raman spectra of purified dermatan and heparan sulfate GAGs. (Bottom) The loading plots of the five latent variables from PLSDA of the spectral data from both normal and diseased measurements. Spectral peaks of the most prominent resemblance are indicated by dotted lines.

#151857 - $15.00 USD Received 27 Jul 2011; revised 26 Aug 2011; accepted 29 Aug 2011; published 6 Sep 2011

diseased tissue as compared to normal, while the mean and 1003 cm^{-1} schemes produced a relative mix in GAG peak intensities between the populations. This is likely to cause the difference in diagnostic accuracy, and is an important consideration for future studies.

While the use of excised tissues that were previously frozen is not as desirable as the study of intact, living tissues, the results obtained here demonstrate the Raman technique's capacity to accurately diagnose MPS. By immediately freezing the samples after collection and studying the passively thawed samples within a reasonable time, it is expected that in-vivo measurements would provide comparable diagnostic success [23]. The study of outer ear was selected due to the thin skin covering of a central cartilaginous region, thereby providing relatively simple optical access to a site of GAG accumulation. The outer ear is also a useful target for future clinical studies for the same reasons and because of the easy anatomic access for an optical instrument. While this study utilized ears that had been clipped for ease of experimental study (minimizing restraint, anesthesia, etc.), the Raman technique is easily made portable and employable via fiber optic means, which would allow its noninvasive interrogation of the tissue to be utilized in clinical environments. Further studies are currently underway to characterize the Raman technique's ability to quantify GAG concentrations for possible identification of disease severity and treatment response. These studies will also evaluate different anatomic measurement sites, such that tissue-level interrogation can be performed.

4. Conclusion

Nearly all standard care and research techniques for MPS diagnosis rely on ex vivo analysis of patient fluids including blood or urine. These approaches offer only systemic measurement of the GAGs which accumulate as a process of the disease. In this paper, we have shown that optical spectroscopy can provide accurate diagnosis of MPS by interrogation of intact tissues. The benefits of this approach are its noninvasiveness, lack of fluid handling, and tissue specificity. Furthermore, because of the specific bands of the GAGs that present in the bulk tissue spectra, this approach may offer the ability to quantify GAG concentrations in various tissue volumes. Thus, optical spectroscopy may offer a new, accurate diagnostic and metric of lysosomal storage diseases such as MPS.

Acknowledgments

The authors thank Mr. Anthony D. Rangel for providing the frozen mouse ear samples used in the study, Mr. Hubert E. Nethercott for genotyping the animals, and Dr. Raymond Y. Wang for his input on the manuscript.

#151857 - $15.00 USD Received 27 Jul 2011; revised 26 Aug 2011; accepted 29 Aug 2011; published 6 Sep 2011